Singh et al. 2023. *Int. J. Vehicle Structures & Systems*, 15(1), 139-146
ISSN: 0975-3060 (Print), 0975-3540 (Online)
doi: 10.4273/ijvss.15.1.26

International Journal of Vehicle Structures & Systems
Available online at https://yanthrika.com/eja

Strategic Optimization of Post Weld Heat Treatment for Dissimilar TIG Weldment of P22 and P91 Steels

Bikram Jit Singh[a], Azad Duppala[b], Parmod Kumar[c], Ravish Arora[a] and Shashi Bahl[d]

[a]Dept. of Mech. Engg., MM Engg. College, Maharishi Markandeshwar (Deemed to be University), Mullana, Haryana, India
[b]Dept. of Mech. Engg., Aditya Institute of Tech. and Management, Tekkali, Andhra Pradesh, India
Corresponding Author, Email: duppalaazadin@gmail.com
[c]Dept. of Mech., Central Inst. of Plastics Engg. and Tech., Ahmedabad, Gujarat, India
Email: parmodrtk@gmail.com
[d]Dept. of Mech., I.K. Gujral Punjab Technical University Hoshiarpur Campus, Hoshiarpur, Punjab, India
Email: shashi.bahl@ptu.ac.in

ABSTRACT:

The Gas Tungsten Arc Welding (GTAW) between P22 (2.25Cr-1Mo) and P91 (9Cr-1Mo) steels are quite common in heavy vehicle structures like; railway locomotives and war (or combat) vehicles. After welding, high hardness values of the Heat-Affected Zones (HAZs) of these dissimilar weld joints are possibly obtained. The uneven hardness in HAZ comes from the austenite transformation to Martensite, because of highly uncontrolled cooling rates. The considerable difference in hardness among various zones leads to prior cracking and is bound to failure during high-temperature operations. Therefore, there is a dire need to establish an appropriate Post Weld Heat Treatment (PWHT) to temper the dissimilar weld joints for required durability. The study investigates the microstructure and mechanical properties of various erupted zones of steel, before and after the application of PWHT. Before and after PWHT, weld zone and HAZ in P22 and P91 are mechanically tested and metallurgically examined. Further PWHT is tried to be optimised strategically and statistically, for the least variation in hardness among different zones. So that any failure due to thermal stresses or strains, during normal running conditions can be avoided.

KEYWORDS:

Post weld heat treatment; Dissimilar weld joints; Heat affected zone; Weld pool; Hardness; Two-way ANOVA

CITATION:

B.J. Singh, A. Duppala, P. Kumar, R. Arora and S. Bahl. 2023. Strategic Optimization of Post Weld Heat Treatment for Dissimilar TIG Weldment of P22 and P91 Steels, *Int. J. Vehicle Structures & Systems*, 15(1), 139-146. doi:10.4273/ijvss.15.1.26.

1. Introduction

The addition of alloying elements not only improves the hardenability but also improve the corrosion and oxidation resistance of alloy steels [1]. It not only increases high-temperature properties, but also increases resistance to abrasion. The modified 9Cr-1Mo steel has been developed by the addition of strong carbide/nitride forming elements such as Va and Nb, which is also known as P91 or grade 91 steel. It offers a good combination of high creep strength and ductility over long exposures at high temperatures [2]. The good weldability and microstructural stability over long exposures at elevated temperatures are other attractive features for 2.25Cr-1Mo (or P22) steels. Because of the versatile desired properties of P91 and P22 steels, the joining of these dissimilar steels is unavoidable, while fabricating heavy vehicle structures and in boiler systems of power plants [3]. Whether it may be welding condenser tubes in railway locomotives or heat exchanger tubes in thermal power plants, P91 and P22 dissimilar steel joints cannot be avoided. TIG welding is the most reliable and frequently used procedure for commercial welding in power plant and petrochemical industry [4]. TIG fusion welding remains a major joining process for the manufacturing of steam generator components. Due to large temperature gradients, narrow heat-affected zones (HAZ) are formed in the base metal on either side of the weld-bead [5, 6]. This causes the heterogeneous distribution of microstructure and leads to a large gradient in the strength values across the weld joints. The presence of a soft inter-critical HAZ is often regarded as a weak link and life-limiting region of a weld joint due to its inferior creep strength [7-8].

The inferior creep strength of the inter-critical HAZ results from preferential accumulation of creep deformation coupled with extensive creep cavitation due to micro-mechanistic effects of constrained deformation and development of damage, commonly known as type-IV cracking [9, 7, 10]. Apart from the heterogeneous microstructure across HAZ, many residual stresses are generated due to weld thermal cycle adds to the strength gradient in the weld joint [11]. After TIG welding between P91 and P22 steel alloys, extreme hardness variation, because of HAZs is obtained. Further during water flow in pipes, if un-heat-treated steels will be used, it results in great affinity of hydrogen at dissimilar weld joints and starts its abrupt cracking [12]. P91 HAZ has a higher hardness value than P22 HAZ, because of its

higher harden ability. The interaction between very high hardness microstructure with hydrogen results in crack initiation [13]. Moreover, the residual stresses during welding will not be relieved that can also cause the failure of dissimilar joints [14]. Thus, the hardness variation in base metal, HAZs and welded joint needs to be reduced for reliable performance of fabricated parts. PWHT is helpful to change the phase transformation from Martensite to ferrite and is required to temper the undue thermal stresses and strains. So, an optimized PWHT seems to be the only solution, to create homogeneous microstructure and hardness, all over the welding joint of P91 and P22 materials.

The carbide depletion in P22 weld metal adjacent to the fusion line of P91-P22 dissimilar welds and its effect on the weld strength had been considered [15]. The carbide coarsening and microstructure degradation during service would result in deterioration in creep strength. A range of microscopy techniques, predominantly transmission electron microscopy had been applied to understand the effect of thermal histories on the microstructure of the materials [16]. Pressure equipment in service had to undergo high pressure and stresses [17]. Tammasophon et al [18] studied experimentally the optimal post-weld heat treatment (PWHT) condition of TIG weld joint between P22 (2.25Cr) and P91 (9Cr) steels using Inconel 625 as filler metal. The PWHT at 750°C for 2, 4 and 6 hours was applied to reach the proper microstructure and hardness for high performance in mechanical properties at elevated temperatures [19]. It was found that PWHT provided more homogeneous microstructures after the welding process and reduced hardness differences in welded microstructures [20]. This further could lead to being a decrease in weld cracking and hence most suitable PWHT condition for TIG weld joints erupted at 750°C for 2 hours. This condition provided the minimum hardness of the weld zone between P91 steel and weld metal as well as the minimum hardness difference between P91 and weld-bead [6, 8].

The effect of PWHTs on the evolution of precipitate phases in dissimilar metal welds made between (9% Cr) P91 alloy and (2.25% Cr) T/P24 alloy had been studied [7, 21]. A lot of research [22-27] has been conducted on materials characterization and its optimization by conventional processes. But a little work has been done on the joining of dissimilar alloys by TIG welding and its behavioural investigation after weld heat treatment. Thus, in present work, the joining of P-22 and P-91 steel alloy specimens is done by using TIG welding. Also, the importance of hardness variations among different heat-affected zones is rarely being considered. Micro-structural studies are indispensable for studying micro-hardness behaviours [19]. Lack of optimum PWHT process for P91 and P22 joints had triggered several boilers bursting accidents in past. Quantitative analysis has always had a cutting edge over qualitative one [21, 28], However, statistical analyses have rarely been used to bring any real-world optimization in this sensitive issue of PWHT.

2. Materials and methods

P91 and P22 grade steel pipes (having diameters of 36mm, 6mm thickness and 300mm length) are welded together, the hardness values of HAZ of P91 steel is over 350VHN, due to its martensitic microstructure. P91 steel alloy had the maximum hardness up to 265VHN, while P22 had a maximum of 173VHN. However, the hardness value of P22 HAZ is not more than 350VHN. P91 HAZ had a higher hardness value than P22 HAZ because of its higher hardenability. The interaction between the high hardness microstructure with hydrogen could result in the crack initiation. The hardness is varying dramatically from 173VHN to 350VHN along the same length of pipe sample. This would also trigger cracking from the weaker and softer microstructure, as it interacts poorly with suddenly harder and fine structure, in the presence of high temperature and pressure conditions. After resizing the pipe samples, the welding process is executed by using electrodes ER-90SB9. The hardness was found to be almost uniform for both the alloy steels before welding. The temperature had been raised by preheating and allowed to homogenize at 250°C. For the close monitoring of temperatures, infrared pyrometers are used at the outer surfaces of the pipes. Fig. 1 shows the specimen welded after TIG welding. Table 1 provides a step-by-step comprehensive experimental procedure. The first step is to prepare the sample according to ASME standards. The pipes of dissimilar steels P91 and P22 are welded with TIG welding. After required characterization, zone-wise hardness before and after PWHT would be compared through data distribution curves.

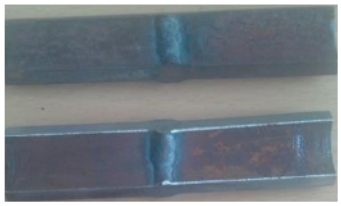

Fig. 1: Specimen fabricated after TIG welding

Table 1: Experimental plan

Steps	Description	Tools / techniques used
1	Welding of dissimilar materials with filler metal	GTAW (TIG) welding
2	Visualizing metallic structures of weld (zone wise)	Optical microscopy
3	Assessing hardness behaviour among various zones (after TIG welding)	VHN hardness tester & one-way ANOVA
4	PWHT (Holding time varies from 8 mins. to 135 mins.)	Sample preparation, Muffle furnace & Two-way ANOVA
5	Prediction of zone wise hardness at shortlisted holding time	Multi-vary chart
6	Demonstration of hardness variation among consecutive zones at optimized holding time	One-way ANOVA
7	Verification of metallic structures (15 samples at optimized holding time)	Sample preparation & Optical microscopy
8	Hardness comparison within the respective zones (before & after PWHT)	Data distribution curve

3. Results and discussion

From the literature survey, it is estimated that five zones namely P22 & P91 base metals, HAZ of P22 & P91 and Weld zone had been generated as described in Fig. 2. For the estimation of microstructural characterization, the samples are prepared and examined respectively by a suitable optical microscope. The microstructure of P22 and P91 base metals (after TIG welding) had polygonal ferrite embedded in bainitic ferrite matrix and tempered Martensite structures, respectively (Fig. 2). The tempered Martensite structure of P91 steel is responsible for its high hardness value. The ferrite structure of P22 steel helped it to maintain good weldability and machinability. The microstructure of P91 HAZ is found to be different from P91 base material. HAZ P91 contained Martensite and retained austenite structures, while HAZ P22 consisted of ferritic bainitic microstructure with finer grains, as compared to its base metal [29, 30]. The change in initial microstructure during welding is responsible for high hardness values of corresponding HAZs formed. Further, the micro-structure of weld pool/bead formed between P91 and P22 grade steels is delineated in Fig. 2. The weld pool comprised of bigger grain sizes of Martensite and retained austenite structures. Some carbide precipitates are also seen in the microstructure, because of chromium and carbon present in austenite phase which reacted further with the atmosphere and made this zone much harder than the others.

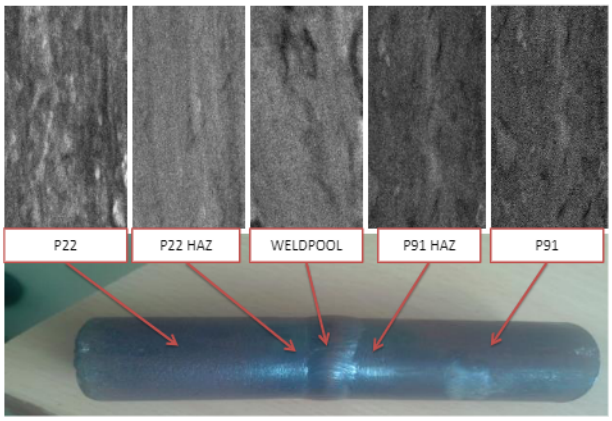

Fig. 2: Optical microstructure at respective zones

After welding, P22 base metal had a polygonal ferrite structure, whereas its HAZ contained ferritic bainitic one. The weld pool possessed Martensite with a large grain size along with retained austenite structure. On the other hand, optical microscopy pinpointed the tempered Martensite structure of P91 base metal and coarse austenite structure of its corresponding HAZ region. After metallographic examination, the Vickers hardness test is carried out at a 10kgf load. All the samples are closely monitored to estimate the hardness of different zones formed during welding.

3.1. Analysis through one-way ANOVA

This statistical test had been conducted by using Minitab-17 software. The purpose of using ANOVA is to investigate the change in hardness among different zones (erupted during TIG welding) with 95% confidence. After calculating a test statistic, the p-value was generated as 0.0001 (<0.05), which implied the quantitatively significant variation in hardness among various zones. The R^2 and R (predicted) were found to be around 90.94% and 90.42% respectively. This signalled about the authenticity of considered independent variables and further deduced the perfect fitness of ANOVA model over the given problem. The box plot is plotted (as elaborated in Fig. 3) where each box represented a middle 50% hardness variation observed in the corresponding zone. The blue dot signified the mean of corresponding samples and found to be 202.417, 310.47, 337.139, 331.917 and 232.444 VHN for P22 base metal, P22 HAZ, weld pool, P91 HAZ and P91 base metal, respectively. Among these, weld pool zone had a maximum mean hardness value, whereas P22 base metal had a least. Outlier is represented by asterisks (*) and is found at 288VHN. The base materials had almost coincided mean and median, but their respective HAZ regions had a large gap. This illustrated the rapid and large variation in hardness at HAZ zones than the welded bead. From the above discussion, it could be predicted with 95% surety that there is a sufficient statistical difference among mean hardness, as far as various zones are in question.

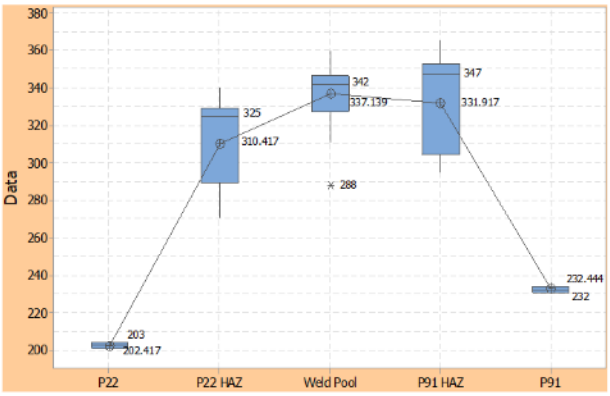

Fig. 3: Zone-wise boxplot

PWHT of 10 samples is done at the various holding times as discussed in the experimental plan. The mean hardness values of different zones after PWHT are encapsulated in Table 2. The first column demonstrated various holding times for 10 samples, while as remaining five columns showed the hardness achieved after PWHT for different zones (i.e. P22 base metal, P22 HAZ, weld pool, P91 HAZ and P91 base metal respectively). Each hardness value is an average of three independent readings at same holding time for corresponding stratas. It is observed that the hardness of all the zones had been decreased after PWHT. But variation among various zones is still to be assessed. This sensitive job is done by applying two-way ANOVA on the spotted data.

Table 2: Region-wise hardness obtained after PWHT

Time (min.)	P22	P22 HAZ	Weld pool	P91 HAZ	P91
8	155	149	180	195	165
15	151	145	185	190	161
30	187	184	214	207	200
45	184	184	206	186	193
60	127	139	175	181	136
75	137	152	181	173	167

90	139	154	169	189	186
105	138	159	171	182	189
120	143	159	183	191	179
135	177	184	171	183	181

3.2. Analysis of hardness through two-way ANOVA

The trends of harnesses obtained after PWHT are analysed by using two-way ANOVA with 5% acceptable error. The hardness analysis is unleashed with respect to region and holding time simultaneously as in Fig. 4. As the generated p-value is found to be less than 0.05 for both the parameters, it signified the importance of these variables as far as hardness is concerned. The mean hardness values (region wise) had been plotted and came out to be least for P22 base metal and maximum for P91HAZ. The mean hardness for different holding times (in minutes) for various samples had been varying from 168.8 to 198.4 VHN. The next outcome of two-way ANOVA is the main effect plots for microhardness as shown in Fig. 5. Minitab created the main effect plot by plotting the hardness mean for both the factors (region and holding time) separately. The hardness first increased sharply with the increase in holding time (from 8 min. to 45 min.) and then decreased abruptly with a further increase in holding time. But after 60 min. of holding, the gradual increment in mean hardness is seen.

Two-way ANOVA: Hardness (VHN) versus Region, Holding Time (in mins)

Source	DF	SS	MS	F	P
Region	4	8463.7	2115.92	17.68	0.000
Holding Time (in mins)	9	8456.5	939.61	7.85	0.000
Error	36	4308.7	119.69		
Total	49	21228.9			

S = 10.94 R-Sq = 79.70% R-Sq(adj) = 72.37%

Individual 95% CIs For Mean Based on Pooled StDev

Region	Mean
P22	153.8
P22 HAZ	160.9
P91	175.7
P91 HAZ	187.7
weld pool	183.5

156 168 180 192

Individual 95% CIs For Mean Based on Pooled StDev

Holding Time (in mins)	Mean
8	168.8
15	166.4
30	198.4
45	190.6

Fig. 4: Two-way ANOVA statistics

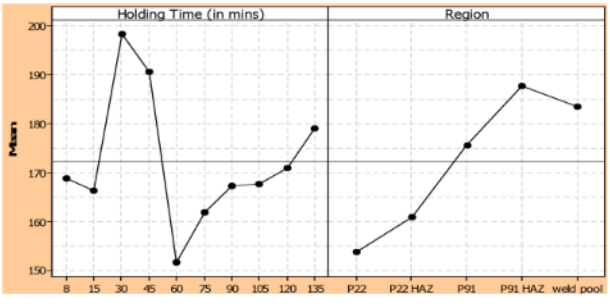

Fig. 5: Main effect plots for hardness w.r.t holding time & region

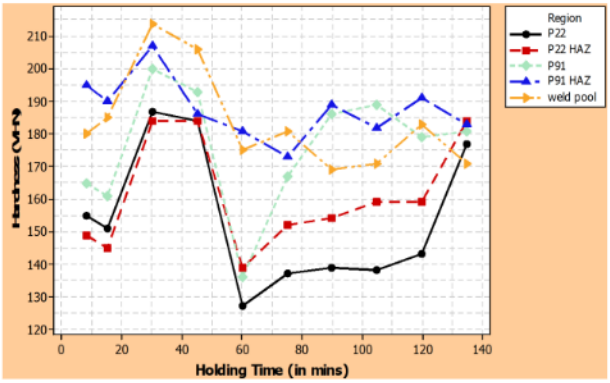

Fig. 6: Scatter plot for hardness vs. Holding time

The lowest mean hardness value is coming at 60 min. of average holding time, whereas the highest is at 30 min. The P22 base metal had the lowest mean hardness (154VHN) but P91HAZ had the highest hardness value (188VHN). After considering both plots concurrently, it had been observed that the overall mean hardness value is impending around 172VHN. Further the cumulative scatter plot for hardness w.r.t. holding times and different zones are delineated (Fig. 6). This graph is predicting the fact that how hardness variation is quite low for P22 base metal and P22 HAZ area, while it has too steep for the region P91 base metal and P91 HAZ, consecutively. The least hardness values are obtained at around 60 and 75 min. of holding time. The scatter plot for the hardness and holding time is depicting the strong linear positive relationship between the two variables. With the help of hardness data acquired after PWHT, a chart is plotted (Fig. 7). The graph contained hardness values along Y-axis and respective regions on X-axis, after PWHT. For representing the different holding times, unique symbols had been used. All the hardness values lied near linear mean square line. It is obvious from the above findings that at a holding time of 68 min. (during PWHT) the individual hardness value of each region had been dropped sufficiently and even the range of hardness variation among different regions is reduced, appreciably. The PWHT is performed at a holding time of 68 min.. Further, data is analysed by using one-way ANOVA to judge the hardness behaviour among different corresponding zones.

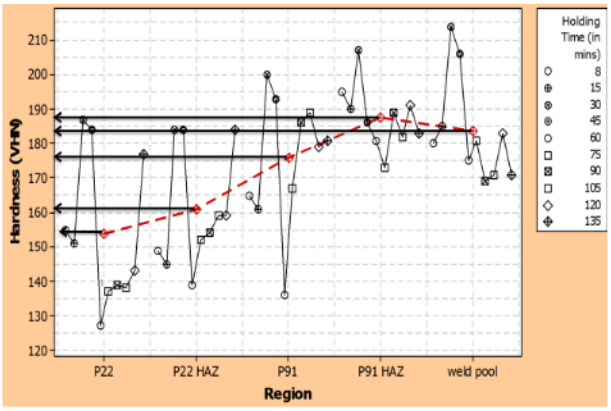

Fig. 7: Multi-vary chart for hardness vs. Distinctive zones

3.3. Behavioural analysis through ANOVA

The tab report had illustrated the f-value as 2.99 with a degree of freedom (DoF) of 4. The R square and R^2

(adjusted) values are estimated as 92.64% and 90.98% respectively. The p-value of 0.095 is determined and is greater than α-level chosen. Hence it could be concluded that there are no quantitatively significant differences existed in hardness of different zones, when PWHT is carried out at 68 min. of holding time (Fig. 8 for complete demonstration). A boxplot is drawn to examine the centre and spread of hardness across various regions. The blue point indicated the mean hardness value of a particular zone and was found to be 172.688, 174.063, 177.813, 176.813 and 175.5VHN for the regions P22 base metal, P22 HAZ, weld pool, P91 HAZ and P91 base metal respectively. The line joining mean hardness values of all the zones remained almost linear, which implied an almost similar hardness range in different regions at 68 min. of holding during PWHT.

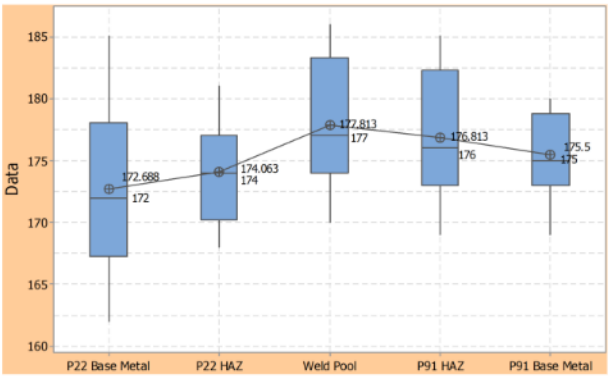

Fig. 8: Boxplot for various zones

To support the results achieved from the hardness tests after PWHT (at average holding time of 68 min.), the samples had further been scrutinized under an optical microscope. Figs. 9(a) and 9(e) represent the microstructures of P22 and P91 base metals after PWHT at 750°C for 68 min. of holding time. There are no optically significant differences in microstructural characteristics detected. However, received micro-structures had tempered Martensite, which consisted of some carbide precipitations near the grain boundaries. Similar characteristics are also unearthed in P22 & P91 HAZ regions, as these had ferrite and ferrite with carbides structures (Figs. 9(b) and 9(d)). Overall, grains became finer after PWHT. Further, the microstructure of the weld zone at Fig. 9(c) is comprised of Martensite matrix with retained austenite, which is quite like the structure of P91 base metal. The value of the carbon mobility at a usual temperature of creep resistant steel (500°C to 700°C), carbon redistribution could be expected during high-temperature exposure of dissimilar metal welds. In the present case, the carbon diffused in the direction of its thermodynamic activity gradient and therefore the two types of areas formed near weld zone i.e. carbon enriched zone (CEZ) and carbon depleted zone (CDZ). The carbon value in P22 steel founded double as compared to P91 steel. Hence, strong redistribution of carbon by diffusion at elevated temperature occurs and distinctive zones of microstructure are formed. The P22 base metal had a tempered Martensite structure with carbide precipitations, but its HAZ zone contained ferritic with carbides precipitation structure.

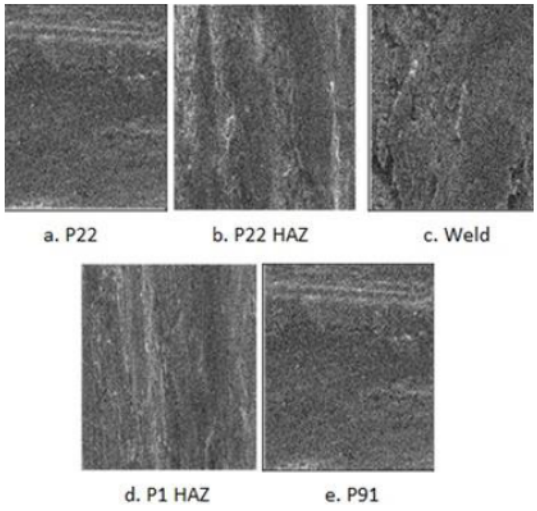

Fig. 9: Optical microstructure w.r.t. zones

The weld pool retained Martensite matrix, whereas P91 HAZ region acquired Martensite with retained austenite structure. An optical microscope also observed the tempered Martensite structure of P91 base metal. For logical deductions, the hardness behaviour for each zone (before and after PWHT) had been evaluated, distinctively. A quantitative comparison is performed after scrutinizing the corresponding data sets. The mean hardness of P22 before PWHT is 202.49VHN and it had effectively reduced to 172.19VHN after PWHT at 68 min. of holding time. A drop of 30.229VHN occurs in the mean hardness value of P22 metal zone. This would cause improvement in brittleness (Fig. 10). The mean hardness value of P22 HAZ before PWHT is 311VHN and it slashed dramatically to 174VHN only. Overall standard deviation decreased from 23.701 to 4.1226 which made the hardness distribution more predictable over HAZ. That's why the spread of the after curve is quite less and restricted as compared to before curve.

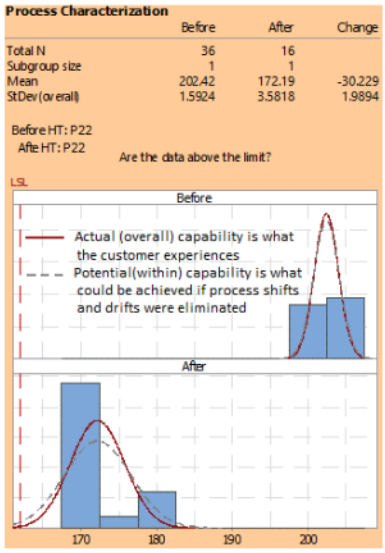

Fig. 10: Hardness comparison for P22 base metal

From p-value it could be visualized statistically that hardness became almost similar for P22 and its HAZ (Fig. 11). The weld pool hardness summary report explained numerically that how hardness is declined

from 326.17VHN to 177VHN after PWHT. The decrement of 148.35VHN is not ignorable accompanied by downsizing in hardness spread (or uncertainty). The p-value spawned is less than 0.05 which signified the effectiveness of PWHT at 68 minutes and brought the hardness of this region around similar to P22 & P22 HAZ (Fig. 12). The comparison chart for P91 HAZ revealed the diminishing trend in hardness from 308.3VHN to 176.81VHN. The standard deviation had also been lowered from 52.0 to 24.5, as supported by the curves graphically. The uniquely designed PWHT had tamed the hardness of both the critical zones and restricted them to around 175VHN (Fig. 13). The PWHT process is well verified by calculating the corresponding p-value. Because it came even less than 0.001, hence the above results could be ascertained (Fig. 14). The major reason for crack development in welded joint is the difference of hardness between P91 HAZ and P91 steel. This is omitted strategically and well-illustrated with PWHT performance report.

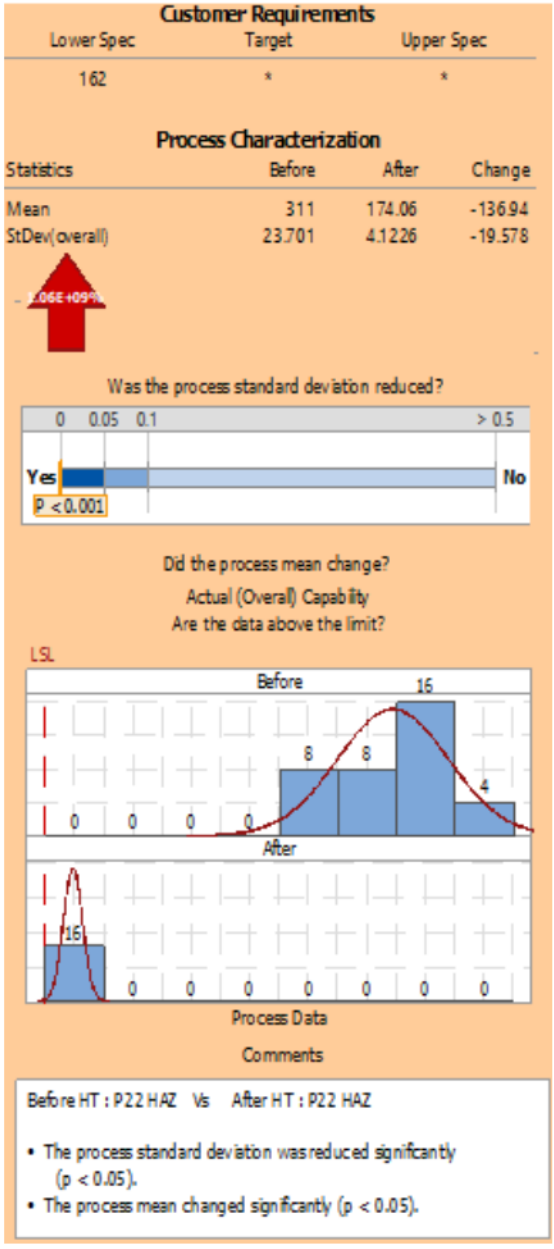

Fig. 11: Hardness comparison for P22 HAZ

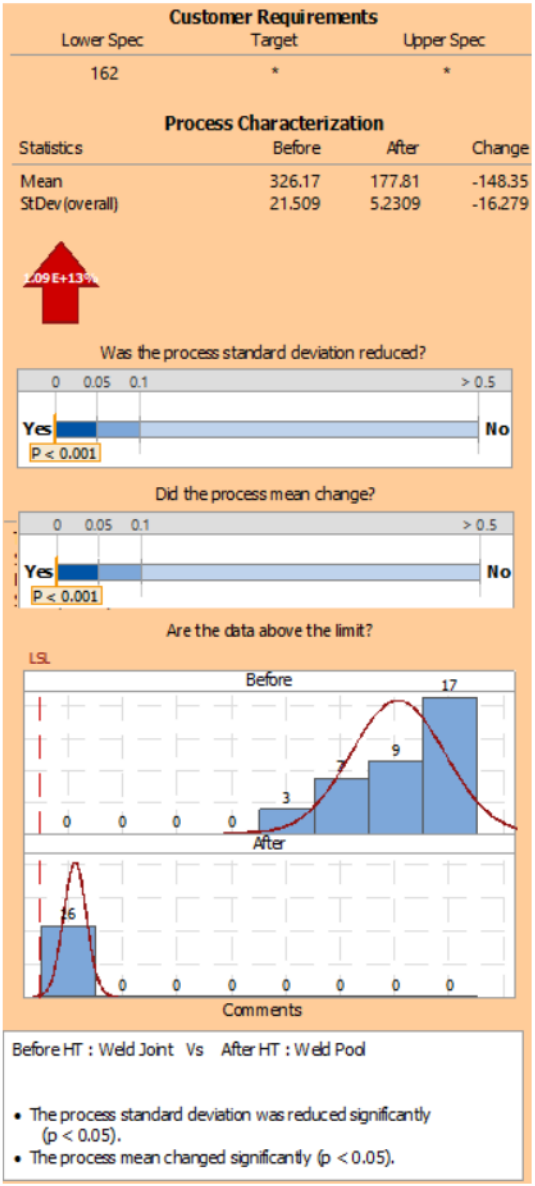

Fig. 12: Hardness comparison for weld pool

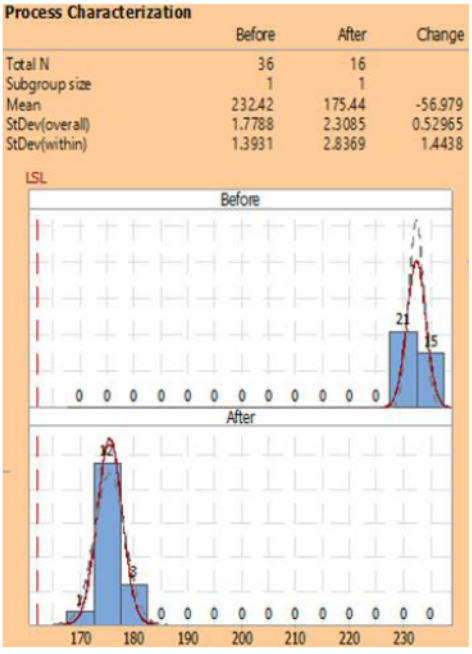

Fig. 13: Hardness appraisal for P91

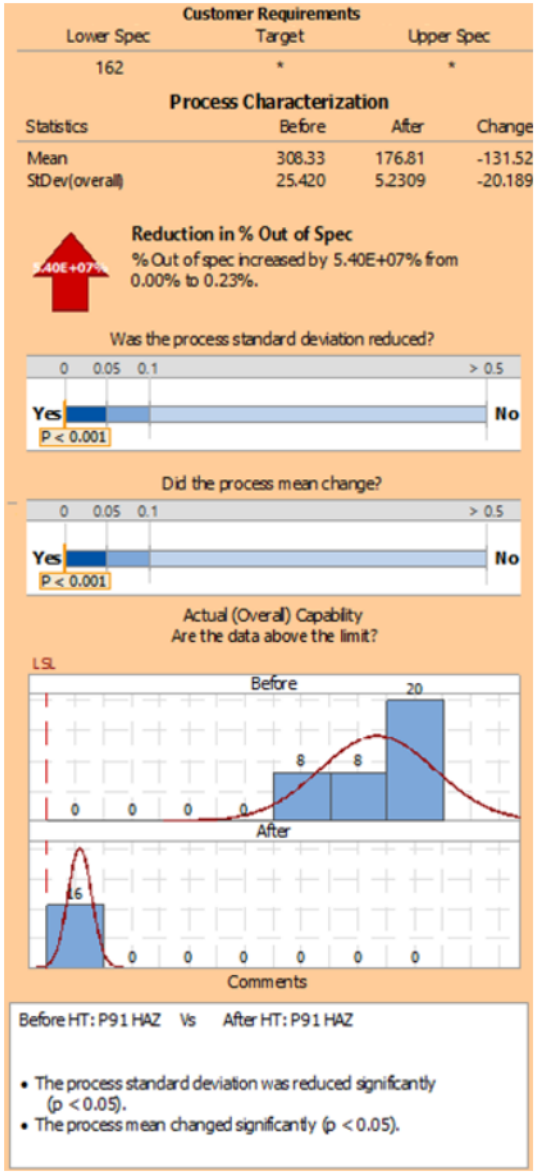

Fig. 14: Hardness evaluation for P91 HAZ

After studying the quoted individual reports, the efficacy of optimized PWHT has been verified and validated. Observations from Figs. 10-14 can deduce quite narrow-range uniformity in hardness, across all the zones. The optimized PWHT is now capable enough to reduce the future risk of joint failure, drastically.

4. Conclusions

From literature, it is concluded that for dissimilar metal welding TIG is almost defect-free and provides suitable strength to the joint. From experiments, it is found that there exists a substantial difference in hardnesses of various zones formed after TIG welding. This has been further verified statistically by using one-way ANOVA. This variation can also be visually inspected by optical microscopy. To overcome this variation in hardness, PWHT is the most suitable process, since it provides more homogeneous microstructures among different zones formed, which could lead to a decrease in weld cracking. The results obtained after PWHT (taking time as a variable) are further analyzed by two-way ANOVA. The homogeneity in microstructures of different zones after PWHT is again validated by optical microscopy. The most suitable PWHT condition for TIG welding of P91 and P22 steel has been evaluated as 750°C with 68.3 min. of holding time. This condition provides the uniform hardness of the weld zone comprised of P91 steel, HAZ P91, P22 HAZ and P22 base metal. The dissimilar weld joints P91/P22 are unstable at temperatures 500°C-900°C from a microstructural point of view. During the high-temperature and long-term exposition, carbon diffuses in the direction of its chemical potential gradient and P22 HAZ and P91 HAZ are formed in weld interface area. The steel with a larger Cr amount is carburized, whereas the steel with lower Cr. The amount is decarburized.

REFERENCES:

[1] M. Allam. 2012. *Investigation on The Influence of Welding Parameters (Heat Input and Heat Treatments) on Weldment Properties of power Boiler Steel P91*, 129-145, Cairo University, Egypt.

[2] D.J. Allen and S.J. Brett. 1999. Premature failure of a P91 header end cap weld: minimising the risks of additional failures, *Proc. Conf. Case Histories in Failure Investigation,* 133-143, Milan, Italy.

[3] B. Arivazhagan, S. Sundaresan and M. Kamaraj. 2009. A study on influence of shielding gas composition on toughness of flux-cored arc weld of modified 9Cr-1Mo (P91) steel, *J. Mat. Processing Tech.*, 209(12/13), 5245-5253. https://doi.org/10.1016/j.jmatprotec.2009.02.006.

[4] A. Kumar, P. Duraisamy and S. Veeramanikandan. 2011. Evaluation of mechanical properties of dissimilar metal tube welded joints using inert gas welding, *Int. J. Engg. Research and Applications*, 2(5), 1709-1717.

[5] J. Baral, J.S. Swaminathan and R.N. Ghosh. 2013. Creep behavior of 9CrMoNbV (P91) steel having a small amount of boron, *Proc. Engg.*, 55, 88-92. https://doi.org/10.1016/j.proeng.2013.03.224.

[6] U. Ceyhan and B. Dogan. 2013. Deformation and fracture behaviour of P91 steel weldments at high temperatures, *Sci. and Tech. Welding and Joining*, 11(5), 538-543. https://doi.org/10.1179/174329306X120705.

[7] P. Chakraborty, P.K. Pradhan, R.K. Fotedar and N. Krishnamurthy. 2012. Compatibility of 9Cr-1Mo steel exposed to thermally convective Pb17Li, *J. Materials Research and Tech.,* 2(3), 206-212. https://doi.org/10.1016/j.jmrt.2013.04.001.

[8] L. Collini, M. Giglio and R. Garziera. 2012. Thermo mechanical stress analysis of dissimilar welded joints in pipe supports: Structural assessment and design optimization, *Engg. Failure Analysis*, 26, 31-49. https://doi.org/10.1016/j.engfailanal.2012.07.002.

[9] C.R. Das, S.K. Albert, J. Swaminathan, A.K. Bhaduri and B.S. Murty. 2013. Effect of boron on creep behaviour of inter-critically annealed modified 9Cr-1Mo steel, *Proc. Engg.*, 55, 402-407. https://doi.org/10.1016/j.proeng.2013.03.271.

[10] S.A. David, J.A. Siefert and Z. Feng. 2013. Welding and weldability of candidate ferritic alloys for future advanced ultra-supercritical fossil power plants, *Sci. and Tech. Welding and Joining*, 18(8), 631-651. https://doi.org/10.1179/1362171813Y.0000000152.

[11] Falat, J. Homolova, M. Kepic and S.A. Vyrostkova. 2012. Microstructure and properties degradation of P/T 91, 92 steels weldment in creep conditions, *J. Mining and*

Metallurgy Section B: Metallurgy, 48(3), 461-469. https://doi.org/10.2298/JMMB120701057F.

[12] Y. Gong, Y. Zhen-Guo and Y. Fa-Yun. 2011. Heat strength evaluation and microstructures observation of the welded joints of one China-made T91 steel, *ASM Int. J. Materials Engg. and Performance,* 21(7), 1313-1319. https://doi.org/10.1007/s11665-011-0048-4.

[13] M.Z. Hamzah, M.L. Ibrahim, Q.H. Chye, B. Ahmad, J.I.I. Hussain, and J. Purbolaksono. 2012. Evaluation on the hardness and microstructures of T91 reheater tubes after post-weld heat treatment, *Engg. Failure Analysis*, 26, 349-354. https://doi.org/10.1016/j.engfailanal.2012.08.019.

[14] Huijun, Li and M. David. 2013. Micro structural characterization of P91 steel in the virgin, service exposed and post-service renormalized conditions, *Steel Research Int.*, 84(12),1302-1308. https://doi.org/10.1002/srin.201300055.

[15] E.I. Samuel, B.K. Choudhary and K.B.S. Rao. 2007. Influence of post-weld heat treatment on tensile properties of modified 9Cr-1Mo ferritic steel base metal, *Material Sci. and Tech.*, 23(8), 992-999. https://doi.org/10.1179/174328407X161295.

[16] Z. Lei, J. Hongyang, X. Lianyong, A. Junchao and X. Guangchun. 2012. Numerical investigation of factors affecting creep damage accumulation in ASME P92 steel welded joint, *Materials and Design*, 34, 566-575. https://doi.org/10.1016/j.matdes.2011.05.009.

[17] G. Qiuzhi, D. Xinjie and L. Yongchang. 2012. Recovery and recrystallization in modified 9Cr-1Mo steel weldment after post-weld heat treatment, *Int. J. Pressure Vessels and Piping,* 93/94, 69-74. https://doi.org/10.1016/j.ijpvp.2012.03.002.

[18] N. Tammasophon, W. Homhragai and G. Lothongkum. 2011. Effect of post weld heat treatment on microstructures and hardness of TIG weldment between P22 and P91 steels with Inconel 625 filler metal, *J. Metals, Materials and Minerals,* 21(1), 93-99.

[19] M.P. Satpathy and S.K. Sahoo. 2017. Parametric analysis on plastic deformation of materials during ultrasonic spot welding with different anvil geometries, *Int. J. Manuf. Tech. and Management*, 31(4), 344-361. https://doi.org/10.1504/IJMTM.2017.10007085.

[20] P. Seliger and A. Thomas. 2006. High temperature behaviour of similar and dissimilar welded components of steel grade P22 and P91, *Proc. 5th Int. Conf. on Mechanics and Materials in Design*, 1-9, Porto, Portugal.

[21] B.J. Singh and Y. Bakshi. 2014. Optimizing the backup power systems through six sigma: A case study of diesel genset, *Int. J. Lean Six Sigma*, 5(2), 168-198. https://doi.org/10.1108/IJLSS-09-2012-0008.

[22] N. Sharma, R.D. Gupta, R. Khanna, R.C. Sharma and Y.K. Sharma. 2021. Machining of Ti-6Al-4V biomedical alloy by WEDM: Investigation and optimization of MRR and Rz using grey-harmony search, *World J. Engg.*, 20(2), 221-234. https://doi.org/10.1108/WJE-05-2021-0278.

[23] R.C. Sharma, V. Dabra, G. Singh, R. Kumar, R.P. Singh and S. Sharma. 2021. Multi-response optimization while machining of stainless steel 316L using intelligent approach of grey theory and grey-TLBO, *World J. Engg.*, 19(3), 329-339. https://doi.org/10.1108/WJE-06-2020-0226.

[24] R. Arora, J. Kapoor and R.C. Sharma. 2021. Development of microwave hybrid heating welded joints of inconel-600 superalloys using grey relational analysis, *Int. J. Vehicle Structures & Systems*, 13(1), 53-59. https://doi.org/10.4273/ijvss.13.1.11.

[25] N. Sharma, W.S. Abduallah, M. Garg, R.D. Gupta, R. Khanna and R.C. Sharma. 2020. Optimization of TIG welding parameters for the 202 stainless steel using NSGA-II, *J. Engg. Research*, 8(4), 206-221. https://doi.org/10.36909/jer.v8i4.7071.

[26] G. Singh, N. Sharma, S. Goyal and R.C. Sharma. 2020. Comparative measurements of physical and mechanical properties of AA6082 based composites reinforced with B 4 C and SiC particulates produced via stir casting, *Metals and Materials Int.*, 27, 4333-4345. https://doi.org/10.1007/s12540-020-00666-0.

[27] N. Sharma, R.D. Gupta, R.C. Sharma, S. Dayal and A.S. Yadav. 2021. Graphene: An overview of its characteristics and applications, *Materials Today: Proc.*, 47(11), 2752-2755. https://doi.org/10.1016/j.matpr.2021.03.086.

[28] B.J. Singh and D. Khanduja. 2011. Does analysis matter in six sigma? A case study, *Int. J. Data Analysis Techniques and Strategies*, 3(3), 300-324. https://doi.org/10.1504/IJDATS.2011.041336.

[29] S. Vani, K. Mariappan, R. Sandhya and M.D. Mathew. 2013. Evaluation of low cycle fatigue damage in grade 91 steel weld joints for high temperature applications *Proc. Engg.*, 55, 128-135. https://doi.org/10.1016/j.proeng.2013.03.231.

[30] A.H. Yaghi, T.H. Hyde, A.A. Becker and W. Sun. 2013. Finite element simulation of welded P91 steel pipe undergoing post-weld heat treatment, *Sci. and Tech. Welding and Joining*, 16(3), 232-238. https://doi.org/10.1179/1362171810Y.0000000018.